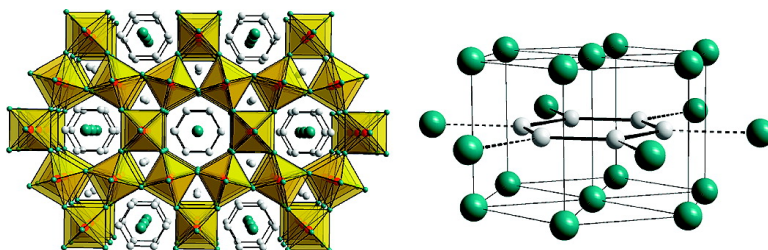


Remarkable Rare-Earth Metal Silicide Oxides with Planar Si Rings

Limin Wang, Zhongjia Tang, Bernd Lorenz, and Arnold M. Guloy

J. Am. Chem. Soc., **2008**, 130 (34), 11258-11259 • DOI: 10.1021/ja803632x • Publication Date (Web): 05 August 2008

Downloaded from <http://pubs.acs.org> on February 8, 2009



More About This Article

Additional resources and features associated with this article are available within the HTML version:

- Supporting Information
- Links to the 1 articles that cite this article, as of the time of this article download
- Access to high resolution figures
- Links to articles and content related to this article
- Copyright permission to reproduce figures and/or text from this article

[View the Full Text HTML](#)



Remarkable Rare-Earth Metal Silicide Oxides with Planar Si₆ Rings

Limin Wang, Zhongjia Tang, Bernd Lorenz, and Arnold M. Guloy*

Department of Chemistry and the Texas Center for Superconductivity, University of Houston,
Houston, Texas 77204-5003

Received May 15, 2008; E-mail: aguloy@uh.edu

Interest on the chemistry of metal-rich compounds has been immense due to their diverse cluster-based structures and novel chemical properties. Alkali metal (Rb, Cs) suboxides underscore the novelty of metal-clusters and metal–metal bonds, in having oxygen atoms enclosed within octahedra of metal atoms. The O-centered octahedra are further linked into discrete clusters.^{1,2} Similarly, these clusters are linked into chains and layers in mixed alkali/alkaline-earth metal suboxides.³ Metal–metal bonds and electronic delocalization dominate the chemical bonding of these suboxides.¹ On the other hand alkaline earth metal-based suboxides are often classified as valence precise Zintl phases.⁴ Examples, include Ba₂₁T₂O₅H₂₄⁵ (T = Ge, Si, In, Tl), Ba₁₀Ge⁷O₃,⁶ M₃EO (M = Ca–Ba and E = Si–Pb),⁷ M₄Pn₂O (Pn = P–Sb).⁸ Rare-earth metal (Ln) analogues of metal-rich suboxides are fewer. Earlier work on the interstitial chemistry of rare-earth metal-based intermetallics led to several oxygen-stabilized interstitial phases derived from well-known intermetallic structure types.⁹ These phases (e.g., La₃AlO_x,¹⁰ Ln₅Pb₃O,¹¹ and La₅Ge₃O_x¹²) accommodate a variety of interstitial atoms that allow the varying of electron counts resulting in modulation of electronic and magnetic properties. The metallic phase, La₉Sb₅O₅, containing O-centered tetrahedral La₄O and square pyramidal La₅O units, is considered a filled-La₂Sb derivative (Sc₂Sb-type) with La-site vacancies.¹³ Interstitial intermetallic compounds are generally described as electron-rich phases, with saturated monatomic or dimeric anions, and their chemical bonding is dominated by metal–metal bonds.⁹

With the wide range of electronic and magnetic properties exhibited by Ln compounds, a search for Ln-rich oxides or suboxides may lead to compounds with new structures, unusual chemical bonding, and properties. More importantly, it provides new directions and creative extensions to the solid state chemistry of Ln-based oxides and polar intermetallics. Herein we report two Ln silicide oxides, La₁₀Si₈O₃ (**1**) and Ce₁₀Si₈O₃ (**2**), that feature the concurrence of strong Ln–Ln bonds and a planar Si₆ Zintl anion analogous to benzene.

The title compounds are best synthesized in high yields by high-temperature reactions (arc-melting) of the pure elements (La pieces, 99.9%; Ce pieces, 99.9%; Si pieces, 99.9999%) under flowing O₂ gas (2.5%) in purified Ar, then arc-annealed under pure argon flow. Nominal oxygen content was varied by the addition of metal oxide precursors and by changing the O₂ concentration or reaction times of the reactions. Compounds **1** and **2** are sensitive to moist air. The lack of appreciable phase widths in **1** and **2** is indicated by the relatively invariant lattice parameters and cell volumes refined from X-ray diffraction patterns of a number of samples with varying nominal metal and oxygen content. Chemical compositions were confirmed by microprobe wavelength dispersive (WDS) studies (Ln₁₀Si_{7.98(2)}O_{3.1(2)}) on bulk and single crystal samples. All manipulations were carried out in a purified Ar-atmosphere glovebox, with total O₂ and H₂O levels <0.1 ppm.

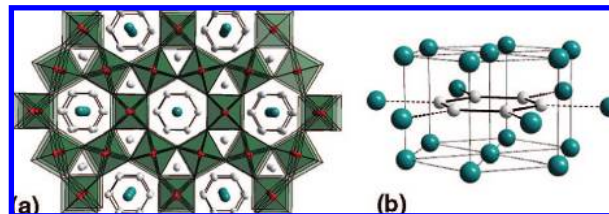


Figure 1. (a) Crystal structure of **1** viewed along [001]. Ln atoms also lie at the vertices of the octahedra. (b) Si₆ unit with its Ln environment. Ln (large blue), Si (medium gray), and O (small red) are shown as spheres.

Small, shiny, silver single crystals of **1** and **2** were isolated from crushed samples for X-ray diffraction analysis.¹⁴ Figure 1 shows the crystal structure of **1** and **2**. It features a hexagonal 3D network of Ln_{6/2}O octahedral, linked via common vertices. Chains of Ln–Si₆–Ln, lie within the hexagonal channels. The LnSi₆-filled hexagonal Ln₃O network is reminiscent of the well-known hexagonal tungsten bronzes, A_xWO₃.¹⁵ This is unprecedented as related rare-earth metal compounds usually crystallize in perovskite-based structures.^{9,10} In **1**, the La₆O octahedral unit is axially compressed with respect to ideal geometry: equatorial and axial La–O distances are 2.846(1) and 2.340(1) Å, respectively. La–La distances range from 3.684(1) to 3.999(1) Å. The large nonspherical O thermal ellipsoids of **1** indicate the O atoms are displaced from the centers of the octahedra owing to the larger volume inside the La₆ octahedra. This is consistent with the well-behaved oxygen thermal ellipsoids in **2**, with smaller Ln atom (Ce). The Si–Si distance in the Si₆ hexagon, 2.379(1) Å, is shorter than Si–Si distances in KSi (2.46 Å),¹⁶ but similar to the Si₆ units in Ba₄Li₂Si₆ (2.382 Å).⁶ The remaining Si atoms (2/formula unit) occupy the center of La₆ trigonal prismatic sites, with La–Si distances ranging from 3.108(1) to 3.337(1) Å. These sites are not occupied in hexagonal tungsten bronzes and partially filled (50% Ge) in Ba₁₀Ge⁷O₃.⁶ Structures of **1** and **2** are different from the analogous binaries, La₅Si₄ and Ce₅Si₄ (Zr₅Si₄-type) which have Si₂ dimers.¹⁷ One may formally associate **1** and **2** with a partial oxidation of the corresponding binaries. However, the presence of the binary phases, at the given reaction temperatures, cannot be ascertained.

Planar Si₆ rings are the principal features of **1** and **2**. A search for arene-like silicides has motivated much research interest on Zintl phases.¹⁸ Si₆ rings found in electron-precise alkaline-earth/alkali metal silicides, assigned as [Si₆]¹⁰⁻, are electron-richer than benzene yet remain aromatic.^{6,18b} Assuming a similar electronic description, and using a Zintl scheme, a plausible charge distribution for **1** is 10La³⁺ = 3O²⁻ + 2Si⁴⁻ + [Si₆]¹⁰⁻ + 6e⁻. However, the validity of the Si₆¹⁰⁻ assignment is questionable considering the availability of a significant “excess” of electrons.

To assess the chemical bonding of the Si₆ rings and to understand the role of orbital-based polar interactions (La–Si) in the electronic structure, full band structure calculations using extended-Hückel (EHT) theory were performed on **1**.¹⁹ Calculated densities of states

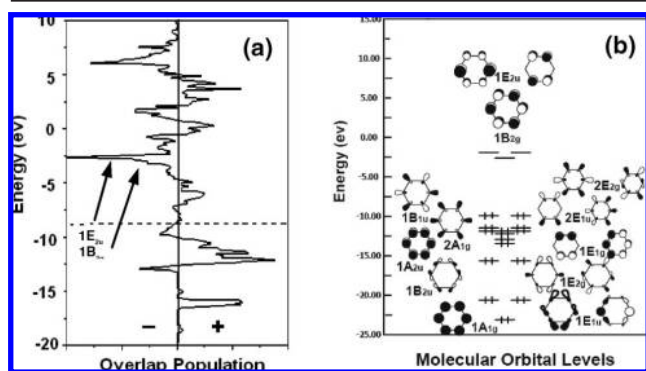


Figure 2. (a) COOP of the Si–Si bonds in **1**; (b) MO diagram of $[\text{Si}_6]^{6-}$.

(DOS), based on 216 k-points, indicate a metallic behavior, with no gaps around the Fermi level (E_F). Bands just below E_F are dominated by La-d states with minor contributions from Si_6 . Unoccupied bands near E_F have significant Si-p character, with some mixing from La states. Furthermore, states associated with the isolated Si atoms lie below E_F , consistent with a Si^{4-} assignment. The important question on the bonding in the Si_6 ring is analyzed using orbital projected DOS, COOP plots, and MO calculations (Supporting Information). These show the Si_6 -derived σ and π bonding states are occupied, and the Si_6 -based π^* states lie essentially above E_F . Calculated MOs correlate well with orbital projection analyses of the band structure. As summarized in Figure 2, the formal electron count of the Si_6 unit is $[\text{Si}_6]^{6-}$, and isoelectronic with benzene. Thus, the electronic scheme is different from $[\text{Si}_6]^{10-}$, previously assigned for the planar Si_6 units in semiconducting $\text{Ba}_4\text{Li}_2\text{Si}_6$ and related phases.⁶

The origin of the lower electron count on Si_6 can be traced to important La– Si_6 “in-plane” interactions. We find that the La–La π -bonding states (1B_{2g} and 1E_{2u}) lie at lower energies than the Si_6 -derived π^* antibonding states (1B_{2g} and 1E_{2u}). Interactions between symmetry equivalent states lead to the stabilization of La–La π -bonding states below E_F , and destabilization of Si_6 π^* states to higher energies above E_F . This is supported by overlap population (COOP) and crystal orbital analyses that show La–Si bonding is optimized at E_F , and the La–Si π^* states having more Si character. Furthermore, “out-of-plane” La– Si_6 interactions, between Si_6 and the closed packed (cp) La atoms that sandwich the La– Si_6 layer (Figure 1b), are negligible. The COOP plots of the La–La interactions also indicate the remaining (cp) La states close to E_F have bonding character, with negligible mixing of Si. However, filling of the La–La bonding states is not maximized (La–La overlap $\approx 0.1/\text{bond}$). Optimized La–Si π interactions and increased cp La–La bonding favors axial compression of the La_6O octahedral, with weak yet optimized La–O bonding. The formal charge distribution is thus: $10\text{La}^{3+} = 3\text{O}^{2-} + \text{Si}_6^{6-} + 2\text{Si}^{4-} + 10\text{e}^-$, with “excess” electrons contributing to significant bonding between reduced La atoms. This is supported by La core binding energies from XPS measurements (Supporting Information).¹²

The validity of our analyses of the EHT results is supported by DFT calculations using the WIEN2K program.²⁰ Calculated DOS obtained from both methods show no band gaps around the Fermi level. In addition, excellent correspondence between orbital states is also observed, with minor differences in absolute energies. Compound **1** exhibits temperature-independent paramagnetism, χ mass susceptibility = $6.69 \times 10^{-5} \text{ emu Oe}^{-1} \text{ g}^{-1}$ (8–300 K), consistent with the predicted metallic behavior. Metallic **2** also

follows a Curie–Weiss paramagnetic behavior ($\theta = -21.2 \text{ K}$) and orders antiferromagnetically at $\sim 7.0 \text{ K}$. Its calculated effective moment, $2.39 \mu_B$, compares well with that of Ce^{3+} ($2.5 \mu_B$).²¹

The new rare-earth metal silicide oxides consist of a metallic suboxide network Ln_{10}O_3 with a hexagonal anti- A_2WO_3 structure and a “Zintl or molecular” part of Si^{4-} and planar Si_6^{6-} anions. The description agrees well with the electronic structures and measured properties. Structural stabilities of the remarkable phases are rationalized by optimized Ln–Si and Si–Si π bonds.

Acknowledgment. This work was supported by the NSF (Grant CHE-0616805), the R. A. Welch Foundation, and the State of Texas through TcSUH.

Supporting Information Available: X-ray crystallographic data in CIF format; results of band calculations; magnetic susceptibility plots; atomic parameters used in calculations; XPS results. This material is available free of charge via the Internet at <http://pubs.acs.org>.

References

- (1) Simon, A. *Alkali and Alkaline Earth Metal Suboxides and Subnitrides. Molecular Clusters of the Main Group Elements*, Wiley-VCH Verlag: Weinheim, Germany, 2004; p 246.
- (2) (a) Karpov, A.; Jansen, M. *Angew. Chem., Int. Ed.* **2005**, *44*, 7639. (b) Karpov, A.; Jansen, M. *Chem. Commun.* **2006**, 1706.
- (3) Vajenine, G. V.; Simon, A. *Angew. Chem., Int. Ed.* **2001**, *40*, 4222.
- (4) (a) Schaefer, H. *Annu. Rev. Mater. Sci.* **1985**, *15*, 1. (b) von Schnering, H. G. *Nova Acta Leopold.* **1985**, *59*, 165.
- (5) (a) Huang, B.; Corbett, J. D. *Inorg. Chem.* **1998**, *37*, 1892. (b) Rohr, C. Z. *Anorg. Allg. Chem.* **1995**, *621*, 1496.
- (6) (a) Schnering, H. G. v.; Bolle, U.; Curda, J.; Peters, K.; Carrillo-Cabrera, W.; Somer, M.; Schultheiss, M.; Wedig, U. *Angew. Chem., Int. Ed. Engl.* **1996**, *35*, 984. (b) Cardoso Gil, R.; Carrillo-Cabrera, W.; Schultheiss, M.; Peters, K.; von Schnering, H. G.; Grin, Yu. *Z. Anorg. Allg. Chem.* **1999**, *625*, 285.
- (7) (a) Widera, A.; Schafer, H. *Mater. Res. Bull.* **1980**, *15*, 1805. (b) Huang, B.; Corbett, J. D. *Z. Anorg. Allg. Chem.* **1998**, *624*, 1787.
- (8) (a) Schaal, H.; Nuss, J.; Hönle, W.; Grin, Yu.; von Schnering, H. G. *Z. Kristallogr.—New Cryst. Struct.* **1998**, *213*, 15. (b) Cardoso-Gil, R.; Nuss, J.; Grin, Yu.; Hönle, W.; von Schnering, H. G. *Z. Kristallogr.—New Cryst. Struct.* **1998**, *213*, 14. (c) Burkhardt, U.; Wied, M.; Hönle, W.; Grin, Yu.; von Schnering, H. G. *Z. Kristallogr.—New Cryst. Struct.* **1998**, *213*, 13.
- (9) Corbett, J. D.; Garcia, E.; Guloy, A. M.; Hurng, W.-M.; Kwon, Y.-U.; Leon-Escamilla, E. A. *Chem. Mater.* **1998**, *10*, 2824.
- (10) Kirchner, M.; Gaebler, F.; Schnelle, W.; Wagner, F. R.; Niewa, R. *Z. Kristallogr.* **2006**, *221*, 543.
- (11) (a) Guloy, A. M.; Corbett, J. D. *Z. Anorg. Allg. Chem.* **1992**, *616*, 61. (b) Macaluso, R. T.; Moreno, N. O.; Fisk, Z.; Thompson, J. D.; Chan, J. Y. *Chem. Mater.* **2004**, *16*, 1560.
- (12) (a) Guloy, A. M.; Corbett, J. D. *Inorg. Chem.* **1993**, *32*, 3532. (b) Guloy, A. M.; Corbett, J. D. *Inorg. Chem.* **1996**, *35*, 4669.
- (13) (a) Nuss, J.; von Schnering, H. G.; Grin, Yu. *Z. Anorg. Allg. Chem.* **2004**, *630*, 2287. (b) Nuss, J.; Jansen, M. *Acta Crystallogr.* **2007**, *B63*, 843.
- (14) Crystal structure data for **1** (**2**): space group $P6/mmm$ (No. 191); $a = 10.975(3) \text{ \AA}$ (10.844(1)); $c = 4.680(1) \text{ \AA}$ (4.561(1)); $Z = 1$; $V = 488.3(2) \text{ \AA}^3$ (464.5(1)); ρ_{calc} = 5.652 g cm^{-3} (5.985); $\mu = 21.828 \text{ mm}^{-1}$ (24.454); $\lambda = 0.71073 \text{ \AA}$ (Mo K α); $2\theta_{\text{max}} = 56.54$; total reflns = 3005 (2865); independent reflns = 269 (275); observed ($I > 2\sigma(I)$) = 247 (256); total variables = 20; ($I > 2\sigma(I)$): $R1 = 0.0125$ (0.013), $wR2 = 0.026$ (0.029), $\text{GOF} = 0.996$ (1.115); all data: $R1 = 0.0144$ (0.0143), $wR2 = 0.027$ (0.029), $\text{GOF} = 0.996$ (1.115). Data collected using a Siemens SMART diffractometer ($T = 25^\circ\text{C}$). Structure was solved by direct methods and refined by full-matrix least-squares calculations.
- (15) (a) Gerand, B.; Nowogrocki, G.; Guenot, J.; Figlarz, M. *J. Solid State Chem.* **1979**, *29*, 429. (b) Tournoux, M.; Ganne, M.; Piffard, Y. *J. Solid State Chem.* **1992**, *96*, 141.
- (16) Busmann, E. *Z. Anorg. Allg. Chem.* **1961**, *313*, 90.
- (17) (a) Guloy, A.; Corbett, J. D. *J. Solid St. Chem.* **2005**, *178*, 1112. (b) Smith, G. S.; Sharp, A. G.; Johnson, Q. *Acta Crystallogr.* **1967**, *22*, 940.
- (18) (a) Guloy, A. M. *Inorganic Chemistry in Focus III*; Wiley-VCH Verlag: Weinheim, Germany, 2006; p 157. (b) Nesper, R. *Inorganic Chemistry in Focus II*; Wiley-VCH Verlag: Weinheim, Germany, 2005; p 143. (c) Todorov, I.; Sevov, S. C. *Inorg. Chem.* **2004**, *43*, 6490.
- (19) Calculations were performed using the program package: Whangbo, M.-H.; Ren, J.; Weigen, L., *CAESAR 1.0*; NCSU: Raleigh, NC, 1998.
- (20) Blaha, P.; Schwarz, K.; Madsen, G.; Kvasnicka, D.; Luitz, J. *Comput. Mater. Sci.* **2003**, *28*, . (WIEN2K)
- (21) Gordon, R. A.; DiSalvo, F. J.; Pöttgen, R.; Brese, N. E. *J. Chem. Soc., Faraday Trans* **1996**, *92*, 2167.

JA803632X